Estimating Grassland Curing with Remotely Sensed Data

Wasin Chaivaranont[1], Jason P. Evans[1], Yi Y. Liu[1, 2], Jason J. Sharples[3]

[1]ARC Centre of Excellence for Climate Systems Science and Climate Change Research Centre, UNSW, Sydney, 2052, Australia

5   [2]School of Geography and Remote Sensing, Nanjing University of Information Science and Technology, Nanjing, 210044, China

[3]School of Physical, Environmental and Mathematical Sciences, UNSW, Canberra, ACT 2600

Correspondence to: Wasin Chaivaranont (w.chaivaranont@student.unsw.edu.au)

Abstract. Wildfire can become a catastrophic natural hazard, especially during dry summer seasons in Australia. Severity is

10   influenced by various meteorological, geographical, and fuel characteristics. Modified Mark 4 McArthur's Grassland Fire Danger Index (GFDI) is a commonly used approach to determine the fire danger level in grassland ecosystems. The degree of curing (DOC, i.e. proportion of dead material) of the grass is one key ingredient in determining the fire danger. It is difficult to collect accurate DOC information in the field, therefore, ground observed measurements are rather limited. In this study, we used satellite observed vegetation greenness (Normalised Difference Vegetation Index, NDVI) and vegetation water

15   content (Vegetation Optical Depth, VOD) information to improve the accuracy of the DOC estimation. First, a statistically significant relationship is established between selected ground observed DOC and satellite observed vegetation datasets (NDVI and VOD) with an r^2 of 0.67. DOC levels estimated using satellite observations were then evaluated using field measurements with an r^2 of 0.55. Results suggest that satellite based DOC estimation can reasonably reproduce ground based observations in space and time. Comparison with currently available satellite based DOC products shows that our model has a comparable

20   and arguably more balanced performance.

Copyright statement

1. Introduction

25   Wildfire can be responsible for major environmental damage or changes to ecosystems (Cobb et al., 2016; Gazzard et al., 2016; Mistry et al., 2016). One of the important components in determining the severity of wildfire is fuel availability. Wildland fuels can vary considerably, both spatially and temporally (Stambaugh et al., 2011). Various interpretations and characterisations of fuel have been made in past studies as a key contribution to assessing wildfire potential (Hudec and Peterson, 2012; Jurdao et al., 2012; Sharples et al., 2009b; Stambaugh et al., 2011; Yebra et al., 2013). Fuel can also be

30   quantified by its age or time since last fire (Bradstock et al., 2010).

In this study, we focus on the availability of combustible fuel in the aboveground biomass in grassland ecosystems; this fuel availability metric is referred to as the degree of curing (DOC). The DOC is the percentage of dead material in a grassland fuel bed; 100 % indicates a fully cured (dead) grassland fuel complex. The DOC has a direct influence on wildfire development in grasslands, hence, it is an important input for fire danger indices and fire spread models, such as the McArthur Grassland

35   Fire Danger Index (GFDI) (Gill et al., 2010) and the CSIRO grassland fire spread model (Cruz et al., 2015; Kidnie et al., 2015). Generally, fires are unable to spread across grasslands that are less than 50 % cured (Anderson et al., 2011). Though this lower limit has been revised, since a more recent study demonstrated that fire can spread in grassland with DOC as low as 20 % (Cruz et al., 2015). In climatological studies, DOC is often assumed to be 100 % (Pitman et al., 2007). This leads to an

overestimation of areas experiencing high levels of fire danger and hence provides only a weak indication of where to focus resources of fire agencies. An accurate, spatially and temporally explicit, estimate of DOC would provide more useful guidance to these agencies.

Measuring DOC in the field is a tedious and expensive task, especially when an accurate assessment of curing is required.
5 Anderson et al. (2011) suggested that current methods for measuring DOC still present problems. The visual assessment method, which relies on field observers to estimate the general curing value based on their expertise and a visual guide, is subjective and can often be unrepresentative of DOC of the entire area. Destructive sampling approaches can provide accurate field based observation, but is a labour intensive task. Thus, Anderson et al. (2011) offered a simple field based method utilising a levy rod, based on the modified point quadrant method of pasture assessment; the approach involves counting the
10 number of live and dead touches on a thin steel rod that was driven into the ground. It was suggested that this approach can be applied across Australia with higher accuracy than current visual assessment methods (Anderson et al., 2011).

Apart from ground measurement, DOC can be estimated using satellite remotely-sensed data, but it is limited by the satellite sensors' capability, e.g. spatial resolution and various atmospheric interferences. Dilley et al. (2004) established a relationship between curing and Normalised Difference Vegetation Index (NDVI, a proxy of vegetation canopy greenness) by estimating
15 live fuel moisture content from NDVI and relating it to curing via an exponential function using a finite difference Levenberg—Marquardt method (Dilley et al., 2004; Rouse et al., 1973). Newnham et al. (2011) showed that estimation of curing using a relative greenness (RG) approach that was based on NDVI distribution provided more accurate estimation of curing than a direct linear regression between curing and NDVI. (Chladil and Nunez, 1995) used curing derived from a soil dryness index model and NDVI to predict soil and fuel moisture content. Various optical based vegetation indices computed from remote
20 sensing reflectance products can also be developed into a satellite based model integrated with ground observations to predict curing (Martin et al., 2015; Turner et al., 2011). These methods, though vastly different in their approaches, achieved good results for their set objectives, but they tend to focus on particular applications. It should also be noted that optical based remote sensing products, including NDVI, are affected by cloud cover and aerosols. Some studies explicitly acknowledge challenges presented by cloud effects and when there are both forest and water bodies in the same NDVI pixel, which results in an
25 erroneous grassland interpretation (Allan et al., 2003; Chladil and Nunez, 1995).

Currently, there are satellite based DOC products over Australia provided by Bureau of Meteorology. The products have 500 m spatial resolution and 8 day temporal resolution, and are based on two past studies (Martin et al., 2015; Newnham et al., 2010). There are five separate satellite based DOC models; four are from Newnham et al. (2010) and one is from Martin et al. (2015). All satellite based DOC models here are based on optical and near-infrared wavelength bands. We aim to improve the
30 DOC estimation over Australia by including a recent passive microwave based satellite product into our analysis.

A passive microwave based remote sensing vegetation product, referred to as Vegetation Optical Depth (VOD), has been developed recently (Meesters et al., 2005). VOD is primarily sensitive to vegetation water content, including both leafy and woody components (Guglielmetti et al., 2007; Jackson and Schmugge, 1991; Kerr and Njoku, 1990). Unlike the traditional optical based vegetation indices, such as NDVI, VOD is minimally influenced by the atmospheric conditions due to its longer
35 wavelength and stronger penetration capacity (Jones et al., 2009). However, it has a coarser spatial resolution (0.1°) in comparison with optical based products, which is a consequence of the low energy microwave emissions from the Earth's surface. It has been demonstrated that VOD can capture the changes in vegetation water content over different land cover types at the global scale, including grassland, cropland, savannas, tropical forests, and boreal forests (Liu et al., 2013a, 2013b, 2015). Also, NDVI and VOD provide complementary information and can comprehensively characterise vegetation dynamics when
40 combined (Andela et al., 2013).

There are two objectives of this study. The first is to improve the estimate of DOC in grasslands by integrating NDVI (vegetation greenness) and VOD (vegetation water content). The second is to implement the improved DOC into GFDI to investigate whether better fire severity predictions can be achieved in grassland environments.

2. Materials

2.1 Satellite based Products

The NDVI dataset used here is derived from the Moderate Resolution Imaging Spectroradiometer (MODIS) 8 day surface reflectance product (MOD09A1) on-board the Terra satellite (Vermote and Vermeulen, 1999). The MOD09A1 product used

5   here for computing NDVI is an 8 day product, which has less noise than the daily product, and its spatial resolution is 0.005° (~500 m). This product is obtained from Remote Sensing at National Computational Infrastructure (NCI) MODIS Land Product for Australia website (Paget and King, 2008). It is produced from original tiles provide by the United States Geological Survey (USGS) for Australia with a starting date from February 18th, 2000.

The 8 day NDVI data is derived from the MODIS reflectance dataset using the following Eq. (1):

10   $$NDVI = \frac{\rho_2 - \rho_1}{\rho_2 + \rho_1} \qquad\qquad (1)$$

where ρ_1 and ρ_2 are spectral reflectance measurements obtained from the visible (red) and near-infrared regions, respectively. During the conversion, to ensure the quality of data, only pixels with ideal quality in all bands and a view angle zenith of less than 60° were kept for the analysis, as suggested by Newnham et al. (2011). The spatial resolution is kept at 0.005°.

The VOD dataset used here is retrieved from the Advanced Microwave Scanning Radiometer – Earth Observing System

15   (AMSR-E) using the Land Parameter Retrieval Model (LPRM) (Meesters et al., 2005; Owe et al., 2001). It has a spatial resolution of 0.1° (~10 km) and nearly daily temporal resolution (Parinussa et al., 2014). The time period covered by AMSR-E is from 2 June 2002 to 3 October 2011, but we used a 9 year range from 4 July 2002 to 26 June 2011 in our analysis by excluding the beginning and the end of the AMSR-E records. The same time period is also used for the MOD09A1 NDVI dataset.

20   VOD data, which has a near daily temporal resolution, is converted to an 8 day average product to reduce noise and ensure complete coverage over Australia (10° S to 45° S and 110° E to 160° E) per temporal interval. The grid cells with radio frequency interference (RFI) are excluded from our analysis. RFI is caused by man-made transmitters, such as radars and wireless communications. These transmitters can be operated in the same frequency range as passive microwave observation, including VOD. Thus, natural signals captured by passive microwave observations are sometimes contaminated with RFI (Nijs

25   et al. 2015).

An example comparison time series of VOD and NDVI from July 2002 to June 2011 at one of the observed DOC sites, Silent Grove, WA (17.131° S, 125.374° E) can be seen in Fig. 1. It is shown that both VOD and NDVI have a similar seasonal cycle. Vegetation types that are present within the VOD (0.1°) and NDVI (0.005°) pixel influence the differences in VOD and NDVI behaviour. The difference between VOD and NDVI spatial resolution can be clearly seen in the example 2° by 2° spatial maps

30   around the Silent Grove area (Fig. 1). We use both VOD and NDVI together to combine their strengths.

The global 0.05° land cover map based on the MODIS MCD12C1 product is used for classifying the dominant land cover type within each VOD pixel. The land cover classification system is as proposed by the University of Maryland (UMD scheme) (Hansen et al., 2000). Figure 2 shows the 0.05° land cover type map of Australia, with observed curing sites marked with crosses. The land cover map used here is from year 2010.

35   A burned area product from MODIS is acquired for further evaluation of the recalculated GFDI from satellite based DOC results. The monthly archived MODIS burned area map reprojected for Australia is obtained from Remote Sensing at the NCI site (Paget and King, 2008). There are two separate MODIS burned area products: the MCD45A1 and the MCD64A1. The MCD64A1 burned area product is preferred over MCD45A1, since it was proven to be more accurate (Andela and van der Werf, 2014; Padilla et al., 2015; Ruiz et al., 2014). Its spatial specification is exactly the same as the MODIS reflectance

40   dataset, with temporal availability from August 2000 onwards. To ensure high quality of the burned pixels, only pixels with the valid data flag from the provided quality control file are included in the analysis. Over 99 % of pixels from mid-2002 to mid-2011 are classified as unburned.

2.2 Ground Based Curing Observations

The observed grassland DOC data was provided by Bushfire and Natural Hazards Cooperative Research Centre and its partner agencies [Project reference: http://www.bushfirecrc.com/projects/a14/grassland-curing]. The observed data were collected from several sites across Australia and New Zealand, ranging from August 2005 to March 2009, usually during summer (Fig. 2). Selected sites were intended to represent broad coverage of major grassland types. Note that the number of locations and samples taken were highly dependent on the availability of field observers from fire management agencies; data were collected with inconsistent interval between data collection dates (Anderson et al., 2011). Three types of data collection approaches were used: visual estimation, levy rod method, and destructive sampling. Due to the number and availability of data as well as their accuracy, only observed DOC from the levy rod method was used in this study. Anderson et al. (2011) and Newnham et al. (2011) state that the levy rod measurement is reliable with less than 1 % bias when compared with destructive sampling.

To identify robust relationships between the site observed and remotely sensed DOC, a number of site criteria must be met. Sites meeting these criteria were used for calibration of the VOD and NDVI satellite based DOC models, while all of the valid records were used for evaluation. One major factor in deciding the site selection is the land use properties of the observed DOC site. The 0.05° land cover type map (MCD12C1) is used for classifying the site location land cover (Hansen et al. 2000). Since 0.1° VOD pixel is covered by 2 by 2 0.05° land cover pixels, the corresponding 2 by 2 pixels of land cover type for each observed curing site can be acquired. The land cover type and homogeneity of each observed DOC site can then be determined, where the site is considered to have a homogeneous land cover only if all four land cover pixels corresponding to the VOD pixel are the same. In case of a site with heterogeneous land cover type, the dominant land cover with the most pixels out of four will be considered as the representative land cover. All observed DOC sites can be categorised into the following land cover types: evergreen broadleaf forest, open shrubland, savannas, woody savannas, grasslands, croplands, and urban.

According to the land use information for each 0.1° VOD pixel, sites identified as evergreen broadleaf forest pixels were removed from the analysis. There are three out of 37 sites situated in the evergreen broadleaf forest, which are Darnum, Simcocks, and Neerim South. Even though actual locations of all observed curing sites were in grassy areas, the VOD signal is a mixture of grassland and forest when the sites are surrounded by dense forests within the same 0.1° pixel.

All sites were also examined to ensure a negative correlation between VOD and the in situ DOC data. That is, since VOD is a proxy for water content in above ground biomass, an overall negative correlation between VOD and curing is expected. If this is not the case, then there is likely some other activity within the 0.1° pixel that disrupts this basic relationship; this effect was found in three sites (Durran Durra, Monaro, and Parry Lagoons). These three sites are also found to be insignificantly correlated with NDVI. Thus, six out of 37 sites are excluded from the analysis.

In addition, there are eight sites (Umbigong, Kilcunda, Tooradin, Tooradin North, Caldermeade Park, Kaduna Park, Hobart Airport, and Jerona) in which VOD data are not available. Most of these are due to sites being located near the coast or a large body of water, where the VOD signal is strongly influenced by the water itself. With the remaining 23 out of 37 sites, several site selection criteria were applied for the calibration phase. The criterion used here to maintain consistency in observation time series requires sites to have at least eight consecutive records, where records are considered consecutive when they are separated by no more than 15 days. Only the consecutive series of records within the selected sites are included in the analysis for the calibration phase. This ensures that the derived model contains the temporal evolution of DOC within years. Only five out of 23 sites are retained for this group, containing a total of 122 observations. Multiple linear regression models of VOD and NDVI were then calibrated with the observed curing from the final selected sites.

2.3 Meteorological Datasets

To further assess the usability of the satellite based curing acquired from the VOD and NDVI model, the GFDI is computed. Additional meteorological data needed for GFDI computation are dry bulb or maximum temperature, 3 pm relative humidity, maximum wind speed, and fuel load (Purton, 1982). Since fuel load is often set as a constant value of 0.45 kg m^{-2} (Sharples et

al., 2009a), there are 3 remaining input datasets needed. These gridded, meteorological datasets are usually derived from the network of ground observation stations across Australia. The range for these datasets is from 4 July 2002 to 26 June 2011 to exactly match with the VOD 9 year range. Both temperature and relative humidity datasets are acquired from the Australian Water Availability Project (AWAP) (Jones et al., 2009). Note that relative humidity is derived from vapour pressure and

5   temperature data. These AWAP datasets have a 0.05° spatial and daily temporal resolution with a coverage region of 10° S to 44.5° S and 112° E to 156° E. For maximum wind speed data, the reanalysis maximum daily wind speed is computed from the ERA–Interim wind components dataset, acquired from the European Centre for Medium–Range Weather Forecasts (ECMWF) (Dee et al., 2011). The reanalysis wind components dataset is available globally at approximately 0.8° spatial resolution at a 6 hour interval.

10   **3. Methods**

3.1 Developing VOD NDVI based dynamic DOC estimates

As indicated by past studies (Dilley et al., 2004; Peterson et al., 2008), NDVI has a significant relationship with live fuel moisture content and DOC. In addition, the NDVI dataset has a spatial resolution of 0.005°. Thus, we investigate whether VOD adds any information to satellite based DOC beyond that embodied in the NDVI through the use of a multiple linear

15   regression model. In addition, a past study suggested that a modified form of NDVI, referred to as relative greenness (RG), has stronger relationship with DOC than NDVI (Newnham et al., 2011). RG can be computed by the following Eq. (2):

$$RG = \frac{NDVI - NDVI_{min}}{NDVI_{max} - NDVI_{min}} \tag{2}$$

where the $NDVI_{min}$ and $NDVI_{max}$ are the minimum and maximum NDVI value over a specified time range. However, given the same observed DOC data and NDVI dataset, we were unable to reproduce a result where the RG correlation with DOC is

20   stronger than NDVI. Further analysis showed that the RG results were very sensitive to the selected time range for the computation, such that results were inconsistent with relatively small differences in the selected range. Due to this, RG is not used in this study and NDVI is used directly in forming a multiple linear regression model to estimate satellite based curing. Some experimentation revealed that the VOD anomalies, computed from the difference between VOD and average VOD over a specified temporal range, yields the best correlation with DOC, but only if the VOD anomalies are computed from the range

25   matching the in situ DOC observation range for each specific site. The range selection for computing VOD anomalies can be quite problematic, since it can heavily influence the correlation result, and no pattern could be found for determining an appropriate VOD range for any other locations outside the observed DOC sites. Thus, we focus our analysis on using the absolute VOD value. The linear regression equation for curing and VOD correlation can be expressed as Eq. (3):

$$C = x_1 + x_2(VOD) \tag{3}$$

30   where x_1 and x_2 are the intercept and slope of the relationship.

Utilising both VOD and NDVI datasets, the following multiple linear regression equation for estimating DOC can be expanded from Eq. (3) as Eq. (4):

$$C = x_1 + x_2(VOD) + x_3(NDVI) + x_4(VOD)(NDVI) \tag{4}$$

where x_1 to x_4 are the intercept and coefficients of VOD, NDVI and the product of VOD and NDVI (interaction term),

35   respectively. Using a stepwise regression, the calibrated final model with corresponding coefficients can be determined. The stepwise fit algorithm used here selects the significant terms with the lowest p-value, which is smaller than the entrance tolerance, to be included in the model first. Next, the algorithm chooses the next most significant term that is still less than the entrance tolerance. This process is repeated until either there are no remaining significant terms or all terms are included in the final model (Draper and Smith, 1998). After the final model is calibrated, we evaluate the DOC model with all valid (23)

40   observed DOC sites.

3.2 Comparing with existing DOC estimates

We acquire existing satellite based DOC products available from Bureau of Meteorology and compare their performance with our model. There are five models available, four are based on Newnham et al. (2010) and one is based on Martin et al. (2015) studies. We decided to test only one of Newnham's models – the one with the best overall RMSE (Method B), and Martin's model (MapVic). Both Method B and MapVic DOC models are as described in Eq. (5) and Eq. (6), as shown below:

$$C_{Method\ B} = 237.31 - 190.14(NDVI) - 142.66(\frac{\rho_7}{\rho_6}) \tag{5}$$

$$C_{MapVic} = 113.80 - 88.41(NDVI) - 67.71(GVMI) \tag{6}$$

where ρ_6 and ρ_7 are spectral reflectance band six and seven from MODIS reflectance dataset and GVMI is Global Vegetation Monitoring Index (Martin et al., 2015; Newnham et al., 2010). GVMI can be calculated by:

$$GVMI = \frac{(\rho_2+0.1)-(\rho_6+0.02)}{(\rho_2+0.1)+(\rho_6+0.02)} \tag{7}$$

where ρ_2 and ρ_6 are spectral reflectance band two and six from MODIS reflectance dataset (Ceccato et al., 2002).

To compare both Method B and MapVic model performance with our model, we evaluate them using the same observed DOC sites. We also computed recalculated GFDI with both Method B and MapVic DOC and assess their burned area prediction capability.

3.3 Comparing GFDI dynamics using different DOC estimates

Several revisions of GFDI were made by past studies (Noble et al., 1980; Purton, 1982). The GFDI revision used in this paper is modified Mark 4 GFDI, since it is the grassland fire danger assessing system that is generally being used by Bureau of Meteorology (Sharples et al., 2009b). Originally, the fire danger rating system was presented in a circular slide rule. A mathematical equation representation of modified Mark 4 GFDI was derived from the circular meter, and can be expressed as follows Eq. (8) (Purton, 1982):

$$GFDI = Q^{1.027}f(C)\exp(-1.523 + 0.0276T_{max} - 0.2205\sqrt{H_{3pm}} + 0.6422\sqrt{V_{max}}) \tag{8}$$

where Q is the fuel load (kg m^{-2}), T_{max} is the dry bulb or daily maximum temperature (° C), H_{3pm} is the daily relative humidity at 3 pm (%), V_{max} is the daily maximum wind speed (km h^{-1}), and $f(C)$ is the curing factor. The curing factor can be calculated by Eq. (9):

$$f(C) = \exp(-0.009432(100 - C)^{1.536}) \tag{9}$$

where C is the grassland DOC (%).

The GFDI is computed on the basis of meteorological input data and either a constant DOC at 100 % or satellite based dynamic curing values. These different GFDI datasets along with the burned area data (MCD64A1) can be used to examine the changes due to variable DOC spatially and temporally. By pairing up burned and unburned pixels with their associated GFDI pixel, we can assess the number of burned and unburned pixels for each GFDI severity level. Using histogram and receiver operating characteristic (ROC) analysis, the difference between original GFDI with constant DOC at 100 % and recalculated GFDI with satellite based dynamic DOC can be assessed (DeLong et al. 1988; Zweig and Campbell 1993).

4. Results

4.1 Comparing VOD-NDVI based and existing DOC estimates

Using the linear model, as described by Eq. (3), Table 1 summarises the curing and VOD correlation result with a significant relationship and an r² of 0.20 with RMSE of 20.80 %.

However, at this level of r^2, VOD alone is not reliable enough to estimate DOC, especially across Australia in general. The study of Newnham et al. (2011) indicated that NDVI alone can perform better at estimating DOC, with an r^2 of approximately 0.50 for a DOC and NDVI linear relationship. The combined explanatory power of NDVI and VOD is explored using a multiple linear regression analysis, as expressed by Eq. (4). The correlation results, along with included terms in the final

5   multiple linear regression model are shown in Table 1. The final model includes the VOD and NDVI interaction (x_4) and NDVI (x_3) terms, and is as shown in Eq. (10). The calibrated r^2 for the final model is 0.67 with RMSE of 13.40 %.

$$C = 145.57 - 260.82(\text{NDVI}) + 137.19(\text{VOD})(\text{NDVI}) \tag{10}$$

The DOC model is then evaluated with all (23) valid observed curing sites. Table 1 also shows the evaluation result, where the evaluated r^2 is 0.55 with RMSE of 15.25 %, which is slightly degraded compared to the calibration performance. With the

10   relatively strong relationship between DOC and VOD and NDVI during calibration and a good robustness in evaluation, the model shown here was chosen for estimating DOC.

These results can be compared to those obtained using existing remotely sensed DOC estimates which are also shown in Table 1. The MapVic DOC has a lower r^2 and higher RMSE, while the Method B DOC has a higher r^2 and lower RMSE when compared with our VOD and NDVI based DOC. This indicates that Method B has the best evaluation among the three models,

15   while MapVic is the worst, and our model sits in the middle between the two. This result is not entirely surprising as all the observations used here were also used in the calibration of Method B (Newnham et al., 2010), a subset is used in the calibration of our method, and MapVic was developed using an independent visual estimates dataset. That is, there is no independent data available for testing Method B, while both our method and MapVic are being tested against independent data.

Using the relationship between VOD, NDVI, and observed DOC (Table 1), we calculated satellite based DOC for Australia.

20   Figure 3 presents maps of satellite based DOC data averaged over the summer periods (December, January, February, DJF) for the years 2002–2003 and 2010–2011. From mid-2002 to mid-2011, the overall average curing for the Australian summer period is the highest during 2003 and the lowest during 2011. Note that the pixels that are classified as any forest types are masked out in white. Comparison time series between satellite based and site observed DOC at Silent Grove, WA (same location as shown in VOD and NDVI example comparison in Fig. 1) is also shown at the top of Fig. 3 as an example.

25   To determine the amount of spatial variation in DOC across Australia, we computed the standard deviation of all valid DOC estimates across the continent within a single time step. The spatial variation time series can then be plotted for the available time period of mid-2002 to mid-2011, as shown in Fig. 4. Note that the continental mean spatial DOC standard deviation is 21.70 %. This indicates that there is significant spatial variability in DOC that persists across all years, and contains a small seasonal component. For a normally distributed variable, 95 % of values would lie within two standard deviations, which is

30   ±43.40 % in this case.

In addition, based on time series of satellite based curing data, Fig. 5 reveals the spatial distribution of standard deviations calculated for each pixel. It shows that most of the strong temporal variation occurs in the south, especially in the southeast and southwest of Australia. Several areas in the midcontinent that have unexpectedly high variation are likely due to rare inundation events. The continental mean temporal standard variation is at 11.88 %. Together, Fig. 4 and Fig. 5 show the

35   variability in DOC that will impact calculations of fire danger indices.

4.2 Comparing GFDI dynamics using different DOC estimates

The spatial plot for maximum summer recalculated GFDI from the DOC multiple linear regression model is shown in Fig. 6, where the top row (a) and (b) are the maps for summer 2003 and summer 2010, respectively. The magnified regions for example fire events in Weston Creek, ACT 2003 and Toodyay, WA 2010 events can be seen in the bottom row (c) and (d).

40   The fire locations are marked with a red crosshair. White pixels are forest areas that were masked using the land cover map. Overall, summer 2003 has 4.51 % more areas indicated as severe or higher GFDI than summer 2010. MCD64A1 burned area map (Fig. 7), also suggested that summer 2003 had 91.45 % more severe wildfire counts than summer 2010. It should be noted

that high GFDI values do not guarantee a fire as there is no accounting for ignition sources, rather a higher GFDI value indicates that if a grassland fire were to start it would spread faster compared to low GFDI values, given no fire suppression activity. Further complicating comparison of Fig. 6 and Fig. 7 is the presence of prescribed burns that are deliberately done during low to moderate GFDI conditions, and that some fires shown in Fig. 7 occur in forested areas where GFDI is not applicable.

5   Nevertheless, they provide a picture of the inter-annual spatial variability in both GFDI and burned area.

The time series plots of recalculated GFDI at Weston Creek, ACT, and Toodyay, WA, for the example 2003 and 2010 fire events were produced, and are shown in Fig. 8. The black line represents the recalculated GFDI from variable DOC, while the dashed, light green line is for original GFDI with constant DOC at 100 %. These locations are marked with red crosshair indicators on the spatial maps (Fig. 6). Note that the original GFDI time series peaks every year, whereas the recalculated

10   GFDI with variable curing time series shows sudden peaks in the days near major fires. The Weston Creek fire was part of the 2003 Canberra bushfire complex, where multiple fires merged and rapidly propagated from 18–22 January 2003, burning 1,600 km^2 (McLeod, 2003). The weather conditions on 18 January 2003 were extreme with temperature as high as 40° C and wind exceeding 60 km h^{-1}. The Toodyay fire was much smaller in magnitude, burning just over 30 km^2 on 29 December 2009. The Weston Creek area is mostly comprised of forest with mixed land cover, whereas the Toodyay area is mostly a mix

15   between croplands and savannas.

Using a burned area observation dataset from MODIS (MCD64A1), we test the effectiveness of GFDI with variable curing in increasing the probability that fires will occur in high GFDI severity levels compared to the probability that fires will occur in low–moderate GFDI severity levels. At each burned and unburned daily data point, the corresponding daily GFDI was calculated. The GFDI histogram in Fig. 9 shows the frequency of satellite based recalculated GFDIs and constant based (DOC

20   = 100 %) reference GFDIs over burned and unburned areas. Figure 9 shows that the recalculated GFDI places the largest percentage of unburned pixels in the low–moderate GFDI severity class, with ~80 % of all unburned pixels occurring in the low–moderate or high severity classes. Meanwhile the reference (DOC = 100 %) GFDI places ~80 % of unburned pixels in the high, very high, severe and extreme classes.

We can evaluate the performance in correctly assigning burned and unburned area for both recalculated and reference GFDI

25   by using the concept of ROC, as described earlier. Assume that the MCD64A1 burned area map represents the true condition and that the GFDI severity level represents the predicted condition, where the prediction is positive when GFDI level is classified as high or above for a burned area and low–moderate for an unburned area. Table 2 shows the contingency table, including both type I (unburned area with high or above GFDI level; false positive) and type II (burned area with low–moderate GFDI level) errors. Though recalculated GFDI has a lower true positive rate of correctly assigning burned area than reference

30   GFDI (0.69 vs 0.88), it is much better at assigning unburned area correctly, i.e. lower false positive rate (0.33 vs 0.52). Overall accuracy for recalculated GFDI is higher than the reference GFDI (0.67 vs 0.48).

Both Method B and MapVic DOC are then used to compute recalculated GFDI and compare with burned area observation dataset in the same manner as our DOC model. From the ROC analysis in Table 3 for Method B and MapVic recalculated GFDI, we found that even though Method B has the best DOC evaluation results (highest r^2, lowest RMSE) and highest overall

35   recalculated GFDI burned and unburned detection accuracy at 0.85, it is the worst at detecting burned area correctly with a true positive rate of only 0.09. This concurs with the findings in Newnham et al. (2010) who found Method B to consistently under predict DOC, and hence it produces fewer cases of high or above GFDI severity. Our model is in the middle ground between Method B and MapVic in terms of overall accuracy.

5. Discussion

5.1 Evaluation of Satellite based DOC

As seen in the results, the final satellite based DOC model has a robust performance when compared with the site observed DOC. In both calibration and evaluation phases, the relationships between the satellite based and observed curing are

5   significant and have r^2 values of 0.55.

Previous studies that derived satellite based DOC have mostly relied solely on NDVI as a predictor. In the study by Newnham et al. (2011) various forms of NDVI were used, including a straight NDVI linear regression and relative NDVI, as shown in Eq. (2). Their results suggested that a linear regression model based on NDVI alone reproduced site observations with an r^2 of 0.50. The results presented here indicate that inclusion of VOD in the regression model yields an improvement in model

10   performance with an increase in the r^2 to 0.55. However, when we compare the evaluation results with the currently available satellite based DOC from Bureau of Meteorology, the best performer is Method B in both r^2 and RMSE (Newnham et al., 2010). We note that this is not a fair comparison as all the data used to evaluate the models was used to calibrate method B. MapVic (Martin et al. 2015), on the other hand, was developed using an independent visual assessment dataset and hence is being evaluated against an independent dataset. While our model used a subset of the data for calibration and the rest of the

15   data provides an independent evaluation.

An earlier study for estimating DOC directly with NDVI yielded even smaller RMSE of up to 6.3 %, but that particular study is focused on data from only three different sites, within a limited study area of 1 km² (Dilley et al., 2004). Older studies that have used NDVI data derived from the National Oceanic and Atmospheric Administration's (NOAA) Advanced Very High Resolution Radiometer (AVHRR) have the same problem of interference from clouds and atmospheric effects, but do not have

20   the advantage of high resolution offered by MODIS (0.05° for AVHRR, but 0.005° for MODIS), or the advantage that VOD is not affected by clouds or aerosol interference.

5.2 GFDI with Various DOC estimates

Though the overall recalculated GFDI from Method B DOC is the best (overall accuracy from best to worst is 0.85 for Method B, 0.67 for our DOC model, 0.61 for MapVic, and 0.48 for GFDI with 100 % constant DOC), we found that it is the worst at

25   detecting burned area correctly (true positive rate from best to worst is 0.88 for GFDI with 100 % constant DOC, 0.74 for MapVic, 0.69 for our DOC model, and 0.09 for Method B). Our VOD and NDVI based DOC model has a good balance in having the second best evaluation result and overall recalculated GFDI accuracy with a decent correct burned area detection rate. We note that GFDI is only an indicator for the level of fire risk, and does not guarantee that a fire will occur, even at an extreme danger level. However, the improvement in accuracy indicates that inclusion of time and space varying curing

30   estimates makes it much more likely that areas identified at a GFDI severity level of high or above will burn than a low–moderate severity level area.

It is worth noting here that in an operational setting atmospheric interference by clouds or smoke will cause gaps in the optical/near-infrared (NDVI) data, while the VOD data remains unaffected. We also note that while the VOD data use here was derived from the AMSR-E sensor which is no longer operational, VOD data derived from currently operating passive

35   microwave sensors, such as Advance Microwave Scanning Radiometer 2 (AMSR2), could be used in an operational setting.

5.3 Limitations

Reducing the chance of incorrectly assigning unburned and burned areas correctly from the ROC analysis made here is purely based on using the burned area map as a true baseline. However, the burned area map may include fires that are deliberately lit in low–moderate conditions, such as prescribed burns and fires that the GFDI is not designed for, such as a fire that burns

in forested regions. The ROC analysis result here is only used to reinforce the idea that using the reference GFDI with constant curing (100 %) leads to overestimating GFDI in some situations, and might result in misleading fire danger warnings.

The satellite based DOC produced here is also at a moderate spatial resolution, which is a limitation of many satellite products. However, DOC in reality can vary over spatial scales much finer than the satellite footprint (less than 500 m^2). As such, our

5   model should only be used as a guide for dynamic, near daily assessment of grassland curing at coarse to moderate spatial scales. This is also true for other satellite based DOC models, including Method B and MapVic models.

6. Conclusions

This study developed an approach to improve the estimation accuracy of degree of grassland curing using a relationship between the observed DOC and satellite based VOD and NDVI. The satellite based dataset was evaluated against the observed

10   DOC data, which resulted in a good fit. Despite the relatively coarse spatial resolution and temporal coverage of VOD and NDVI datasets used in this study, the satellite based curing dataset produced has the potential to contribute to the preparedness of fire management agencies and improve fire spread modelling With a comparable and arguably more balanced performance in correctly detecting burned and unburned area through GFDI than currently available satellite based DOC models (i.e. Method B and MapVic), our model could provide an appealing alternative estimated DOC data for GFDI computations and

15   fire risk modelling.

Data availability

The following datasets and their associated sources or contact points are as listed below:

- MODIS MOD09A1, MCD16C1 and MCD64A1 for NDVI computation, land cover type map, and burned area map for Australia are freely available from NASA via Remote Sensing at NCI: http://remote-

20   sensing.nci.org.au/u39/public/html/modis/lpdaac-mosaics-cmar/

- AMSR-E VOD dataset for Australia is available upon request by contacting Yi Liu: yi.liu@nuist.edu.cn
- Observed DOC dataset via visual assessment, levy rod, and destructive methods is available upon request from the following Bushfire and Natural Hazards Cooperative Research Centre legacy project: http://www.bushfirecrc.com/projects/a14/grassland-curing

25   - Maximum daily observed gridded temperature and vapour pressure dataset for Australia are freely available from AWAP: http://www.bom.gov.au/jsp/awap/

- ERA-Interim maximum daily reanalysis gridded wind components for Australia are freely available from ECMWF: http://www.ecmwf.int/en/research/climate-reanalysis/era-interim

Author contribution

30   Wasin Chaivaranont, Jason Evans, and Yi Liu are involved in initial research planning and experiments design. For the rest of the study, including the analysis of the results, paper writing, and manuscript proofreading, all authors (Wasin Chaivaranont, Jason Evans, Yi Liu, and Jason Sharples) are involved.

Competing interests

The authors declare that they have no conflict of interest.

Acknowledgements

We would like to acknowledge the following parties:

- NASA for making MODIS data freely available.
- NCI for making a freely available preprocessed MODIS data for Australia.
5
- Bushfire and Natural Hazards Cooperative Research Centre and its partner agencies for allowing us to use their observed DOC dataset from their legacy project.
- AWAP for making daily Australia climate gridded dataset freely available.
- ECMWF for making ERA-Interim reanalysis gridded dataset freely available.

References

10 Allan, G., Johnson, A., Cridland, S. and Fitzgerald, N.: Application of NDVI for predicting fuel curing at landscape scales in northern Australia: can remotely sensed data help schedule fire management operations?, Int. J. Wildland Fire, 12(4), 299–308, 2003.

Andela, N. and van der Werf, G. R.: Recent trends in African fires driven by cropland expansion and El Nino to La Nina transition, Nat. Clim. Change, 4(9), 791–795, doi:10.1038/nclimate2313, 2014.

15 Andela, N., Liu, Y. Y., van Dijk, A. I. J. M., de Jeu, R. A. M. and McVicar, T. R.: Global changes in dryland vegetation dynamics (1988–2008) assessed by satellite remote sensing: comparing a new passive microwave vegetation density record with reflective greenness data, Biogeosciences, 10(10), 6657–6676, doi:10.5194/bg-10-6657-2013, 2013.

Anderson, S. A. J., Anderson, W. R., Hollis, J. J. and Botha, E. J.: A Simple Method For Field-Based Grassland Curing Assessment, Int. J. Wildland Fire, 20, 804–814, 2011.

20 Bradstock, R. A., Hammill, K. A., Collins, L. and Price, O.: Effects of weather, fuel and terrain on fire severity in topographically diverse landscapes of south-eastern Australia, Landsc. Ecol., 25(4), 607–619, doi:10.1007/s10980-009-9443-8, 2010.

Ceccato, P., Gobron, N., Flasse, S., Pinty, B. and Tarantola, S.: Designing a spectral index to estimate vegetation water content from remote sensing data: Part 1: Theoretical approach, Remote Sens. Environ., 82(2–3), 188–197, doi:10.1016/S0034-
25 4257(02)00037-8, 2002.

Chladil, M. and Nunez, M.: Assessing Grassland Moisture and Biomass in Tasmania - the Application of Remote-Sensing and Empirical-Models for a Cloudy Environment, Int. J. Wildland Fire, 5(3), 165–171, 1995.

Cobb, R. C., Meentemeyer, R. K. and Rizzo, D. M.: Wildfire and forest disease interaction lead to greater loss of soil nutrients and carbon, Oecologia, 1–12, doi:10.1007/s00442-016-3649-7, 2016.

30 Cruz, M. G., Gould, J. S., Kidnie, S., Bessell, R., Nichols, D. and Slijepcevic, A.: Effects of curing on grassfires: II. Effect of grass senescence on the rate of fire spread, Int. J. Wildland Fire, 24(6), 838–848, doi:10.1071/WF14146, 2015.

Dee, D. P., Uppala, S. M., Simmons, A. J., Berrisford, P., Poli, P., Kobayashi, S., Andrae, U., Balmaseda, M. A., Balsamo, G., Bauer, P., Bechtold, P., Beljaars, A. C. M., van de Berg, L., Bidlot, J., Bormann, N., Delsol, C., Dragani, R., Fuentes, M., Geer, A. J., Haimberger, L., Healy, S. B., Hersbach, H., Hólm, E. V., Isaksen, L., Kållberg, P., Köhler, M., Matricardi, M.,
35 McNally, A. P., Monge-Sanz, B. M., Morcrette, J.-J., Park, B.-K., Peubey, C., de Rosnay, P., Tavolato, C., Thépaut, J.-N. and Vitart, F.: The ERA-Interim reanalysis: configuration and performance of the data assimilation system, Q. J. R. Meteorol. Soc., 137(656), 553–597, doi:10.1002/qj.828, 2011.

Dilley, A. C., Millie, S., O'Brien, D. M. and Edwards, M.: The relation between Normalized Difference Vegetation Index and vegetation moisture content at three grassland locations in Victoria, Australia, Int. J. Remote Sens., 25(19), 3913–3930,
40 doi:10.1080/01431160410001698889, 2004.

Draper, N. R. and Smith, H.: Applied Regression Analysis, 3rd ed., Wiley-Interscience, Hoboken, NJ., 1998.

Gazzard, R., McMorrow, J. and Aylen, J.: Wildfire policy and management in England: an evolving response from Fire and Rescue Services, forestry and cross-sector groups, Phil Trans R Soc B, 371(1696), 20150341, doi:10.1098/rstb.2015.0341, 2016.

Gill, A. M., King, K. J. and Moore, A. D.: Australian grassland fire danger using inputs from the GRAZPLAN grassland simulation model, Int. J. Wildland Fire, 19(3), 338–345, 2010.

Guglielmetti, M., Schwank, M., Mätzler, C., Oberdörster, C., Vanderborght, J. and Flühler, H.: Measured microwave radiative transfer properties of a deciduous forest canopy, Remote Sens. Environ., 109(4), 523–532, doi:10.1016/j.rse.2007.02.003, 2007.

Hansen, M. C., Defires, R. S., Townshend, J. R. G. and Sohlberg, R.: Global land cover classification at 1km resolution using a decision tree classifier, Int. J. Remote Sens., 21, 1331–1365, 2000.

Hudec, J. L. and Peterson, D. L.: Fuel variability following wildfire in forests with mixed severity fire regimes, Cascade Range, USA, For. Ecol. Manag., 277, 11–24, doi:10.1016/j.foreco.2012.04.008, 2012.

Jackson, T. J. and Schmugge, T. J.: Vegetation effects on the microwave emission of soils, Remote Sens. Environ., 36, 203–212, 1991.

Jones, D. A., Wang, W. and Fawcett, R.: High-quality spatial climate data-sets for Australia, Aust. Meteorol. Oceanogr. J., 58(4), 233–248, 2009.

Jurdao, S., Chuvieco, E. and Arevalillo, J. M.: Modelling Fire Ignition Probability from Satellite Estimates of Live Fuel Moisture Content, Fire Ecol., 7(1), 77–97, doi:10.4996/fireecology.0801077, 2012.

Kerr, Y. H. and Njoku, E. G.: A semiempirical model for interpreting microwave emission from semiarid land surfaces as seen from space, IEEE Trans. Geosci. Remote Sens., 28(3), 384–393, doi:10.1109/36.54364, 1990.

Kidnie, S., Cruz, M. G., Gould, J., Nichols, D., Anderson, W. and Bessell, R.: Effects of curing on grassfires: I. Fuel dynamics in a senescing grassland, Int. J. Wildland Fire, 24(6), 828–837, 2015.

Liu, Y. Y., Evans, J. P., McCabe, M. F., de Jeu, R. A. M., van Dijk, A. I. J. M., Dolman, A. J. and Saizen, I.: Changing Climate and Overgrazing Are Decimating Mongolian Steppes, PLoS ONE, 8(2), e57599, doi:10.1371/journal.pone.0057599, 2013a.

Liu, Y. Y., van Dijk, A. I. J. M., McCabe, M. F., Evans, J. P. and de Jeu, R. A. M.: Global vegetation biomass change (1988–2008) and attribution to environmental and human drivers, Glob. Ecol. Biogeogr., 22(6), 692–705, doi:10.1111/geb.12024, 2013b.

Liu, Y. Y., van Dijk, A. I. J. M., de Jeu, R. A. M., Canadell, J. G., McCabe, M. F., Evans, J. P. and Wang, G.: Recent reversal in loss of global terrestrial biomass, Nat. Clim. Change, 5(5), 470–474, doi:10.1038/nclimate2581, 2015.

Martin, D., Chen, T., Nichols, D., Bessell, R., Kidnie, S. and Alexander, J.: Integrating ground and satellite-based observations to determine the degree of grassland curing, Int. J. Wildland Fire, 24(3), 329–339, 2015.

McLeod, R.: Inquiry into the Operational Response to the January 2003 Bushfires in the ACT, ACT Government. [online] Available from: http://pandora.nla.gov.au/pan/35870/20030923-0000/www.cmd.act.gov.au/mcleod_inquiry/Documents/Final/McLeodInquiry.pdf, 2003.

Meesters, A. G. C. A., de Jeu, R. A. M. and Owe, M.: Analytical derivation of the vegetation optical depth from the microwave polarization difference index, IEEE Geosci. Remote Sens. Lett., 2(2), 121–123, doi:10.1109/LGRS.2005.843983, 2005.

Mistry, J., Bilbao, B. A. and Berardi, A.: Community owned solutions for fire management in tropical ecosystems: case studies from Indigenous communities of South America, Phil Trans R Soc B, 371(1696), 20150174, doi:10.1098/rstb.2015.0174, 2016.

Newnham, G., Grant, I., Martin, D. and Anderson, S. A. J.: Improved Methods for Assessment and Prediction of Grassland Curing, Bushfire Cooperative Research Centre., 2010.

Newnham, G. J., Verbesselt, J., Grant, I. F. and Anderson, S. A. J.: Relative Greenness Index for assessing curing of grassland fuel, Remote Sens. Environ., 115(6), 1456–1463, doi:10.1016/j.rse.2011.02.005, 2011.

Noble, I. R., Gill, A. M. and Bary, G. a. V.: McArthur's fire-danger meters expressed as equations, Aust. J. Ecol., 5(2), 201–203, doi:10.1111/j.1442-9993.1980.tb01243.x, 1980.

Owe, M., De Jeu, R. and Walker, J.: A methodology for surface soil moisture and vegetation optical depth retrieval using the microwave polarization difference index, IEEE Trans. Geosci. Remote Sens., 39(8), 1643–1654, doi:10.1109/36.942542, 2001.

Padilla, M., Stehman, S. V., Ramo, R., Corti, D., Hantson, S., Oliva, P., Alonso-Canas, I., Bradley, A. V., Tansey, K., Mota, B., Pereira, J. M. and Chuvieco, E.: Comparing the accuracies of remote sensing global burned area products using stratified random sampling and estimation, Remote Sens. Environ., 160, 114–121, doi:10.1016/j.rse.2015.01.005, 2015.

5   Paget, M. J. and King, E. A.: MODIS Land data sets for the Australian region, Internal Report, CSIRO Marine and Atmospheric Research Black Mountain, Canberra, Australia. [online] Available from: http://remote-sensing.nci.org.au/u39/public/html/modis/lpdaac-mosaics-cmar/, 2008.

Parinussa, R. M., Yilmaz, M. T., Anderson, M. C., Hain, C. R. and de Jeu, R. a. M.: An intercomparison of remotely sensed soil moisture products at various spatial scales over the Iberian Peninsula, Hydrol. Process., 28(18), 4865–4876, doi:10.1002/hyp.9975, 2014.

10   Peterson, S. H., Roberts, D. A. and Dennison, P. E.: Mapping live fuel moisture with MODIS data: A multiple regression approach, Remote Sens. Environ., 112(12), 4272–4284, doi:10.1016/j.rse.2008.07.012, 2008.

Pitman, A. J., Narisma, G. T. and McAneney, J.: The impact of climate change on the risk of forest and grassland fires in Australia, Clim. Change, 84(3–4), 383–401, doi:10.1007/s10584-007-9243-6, 2007.

Purton, C. M.: Equations for the McArthur mark 4 grassland fire danger meters., Meteorol. Note, 147, 1982.

15   Rouse, J. W., Haas, R. H., Schell, J. A. and Deering, D. W.: Monitoring vegetation systems in the Great Plains with ERTS, Third ERTS Symp., 309–317, 1973.

Ruiz, J. A. M., Lázaro, J. R. G., Cano, I. del Á. and Leal, P. H.: Burned Area Mapping in the North American Boreal Forest Using Terra-MODIS LTDR (2001–2011): A Comparison with the MCD45A1, MCD64A1 and BA GEOLAND-2 Products, Remote Sens., 6(1), 815–840, doi:10.3390/rs6010815, 2014.

20   Sharples, J. J., McRae, R. H. D., Weber, R. O. and Gill, A. M.: A simple index for assessing fire danger rating, Environ. Model. Softw., 24(6), 764–774, doi:10.1016/j.envsoft.2008.11.004, 2009a.

Sharples, J. J., McRae, R. H. D., Weber, R. O. and Gill, A. M.: A simple index for assessing fuel moisture content, Environ. Model. Softw., 24(5), 637–646, doi:10.1016/j.envsoft.2008.10.012, 2009b.

Stambaugh, M. C., Dey, D. C., Guyette, R. P., He, H. S. and Marschall, J. M.: Spatial patterning of fuels and fire hazard across 25   a central U.S. deciduous forest region, Landsc. Ecol., 26(7), 923–935, doi:10.1007/s10980-011-9618-y, 2011.

Turner, D., Lewis, M. and Ostendorf, B.: Spatial indicators of fire risk in the arid and semi-arid zone of Australia, Ecol. Indic., 11(1), 149–167, doi:10.1016/j.ecolind.2009.09.001, 2011.

Vermote, E. F. and Vermeulen, A.: Atmospheric Correction Algorithm: Spectral Refelctances (MOD09), 1999.

Yebra, M., Dennison, P. E., Chuvieco, E., Riano, D., Zylstra, P., Hunt Jr., E. R., Danson, F. M., Qi, Y. and Jurdao, S.: A global 30   review of remote sensing of live fuel moisture content fofire danger assessment: Moving towards operational products, Remote Sens. Environ., 136, 455–468, 2013.

Figures and Tables
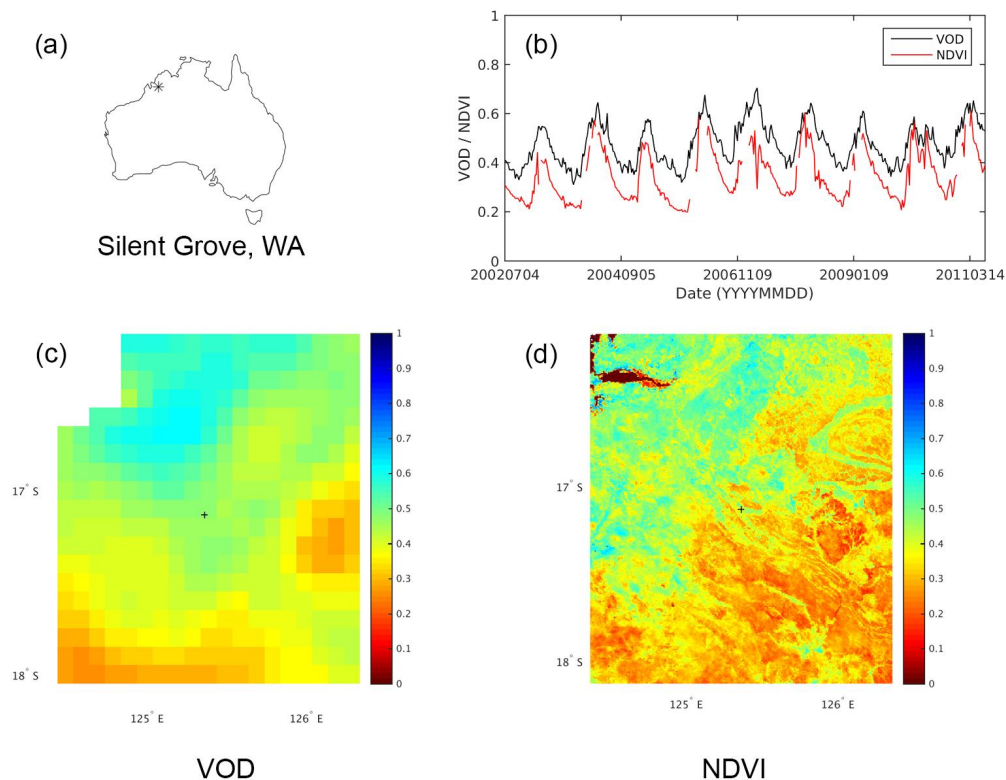
Figure 1: Example Vegetation Optical Depth (VOD) and Normalised Difference Vegetation Index (NDVI) time series (b) and spatial maps, (c) for VOD and (d) for NDVI, at Silent Grove, WA (17.131° S, 125.374° E). The star (*) indicate the location of the time series on Australia map (a).
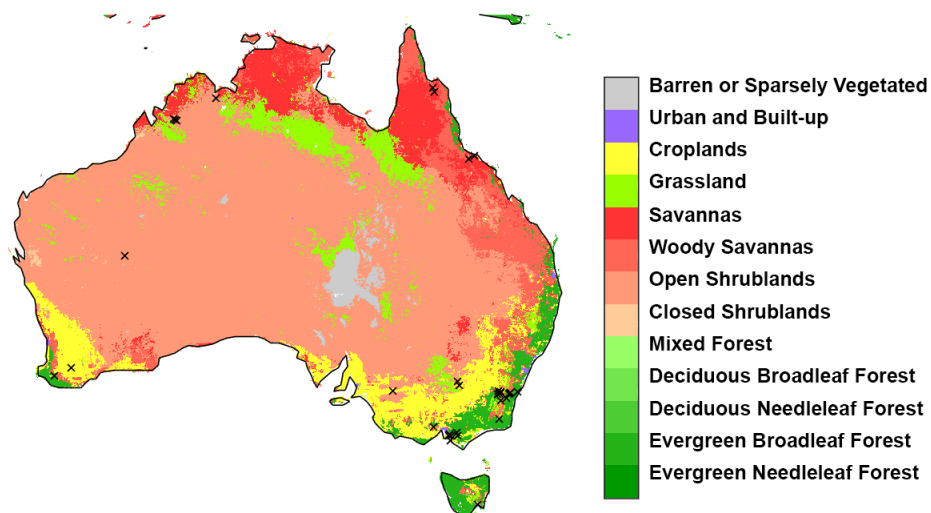
Figure 2: MCD12C1 land cover type map for Australia (Hansen et al., 2000). The locations of observed degree of curing (DOC) sites are marked with crosses.
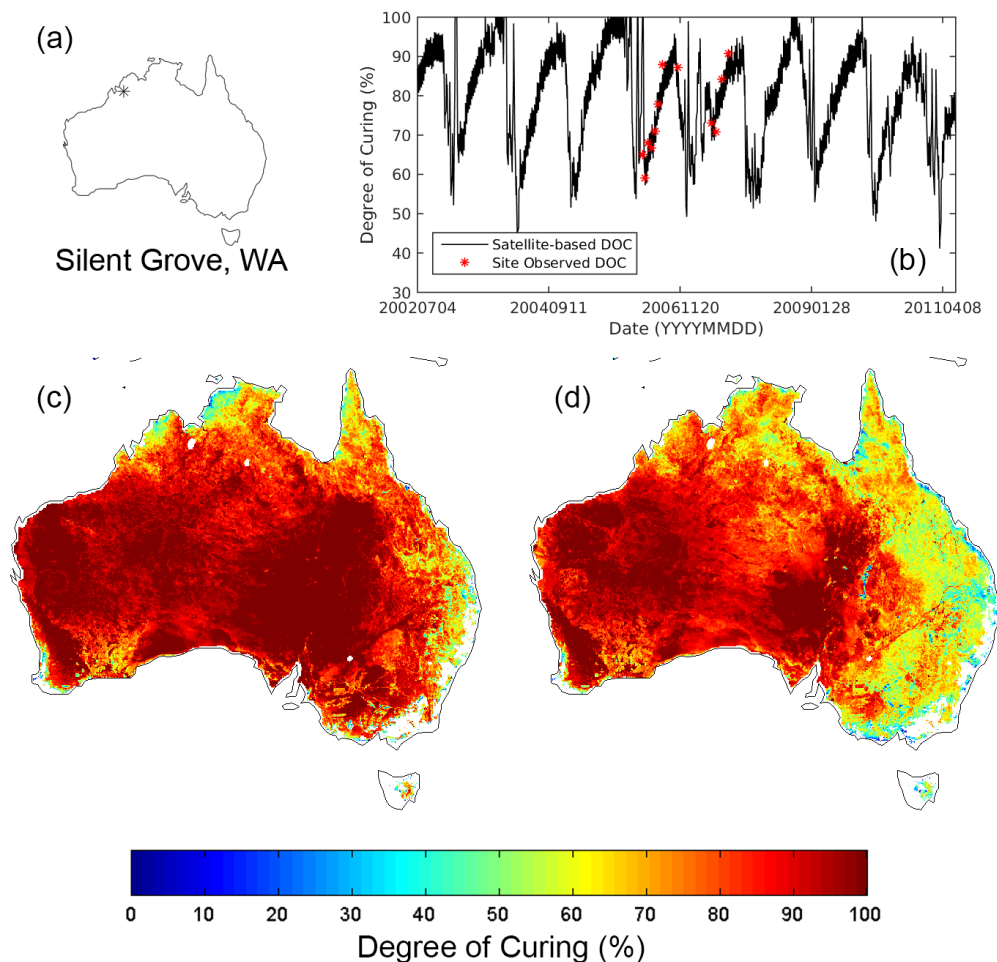
Figure 3: Example satellite based and site observed degree of curing (DOC) time series comparison at Silent Grove, WA (17.131° S, 125.374° E) (b), where the star (*) indicate the location of the time series on Australia map (a). Satellite based DOC across Australia during summer (December, January, February) for 2002—2003 (c) and 2010—2011 (d) are shown with forest areas masked out.
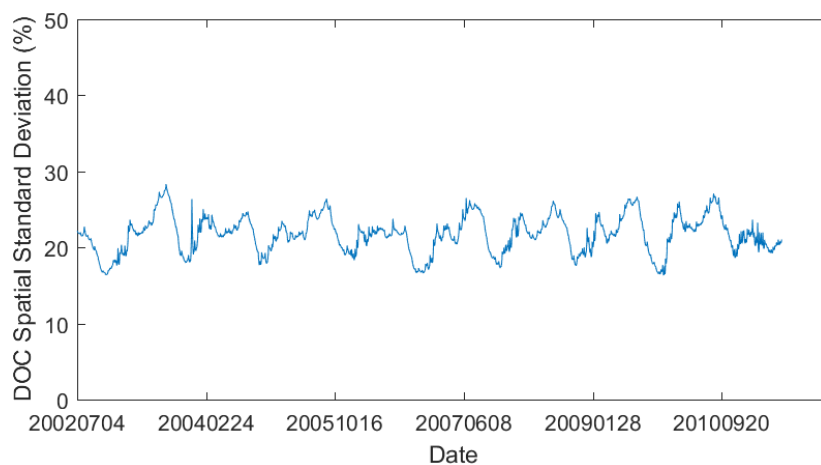
Figure 4: Spatial standard deviation of estimated degree of curing (DOC) time series from 4 July 2002 to 26 June 2011.
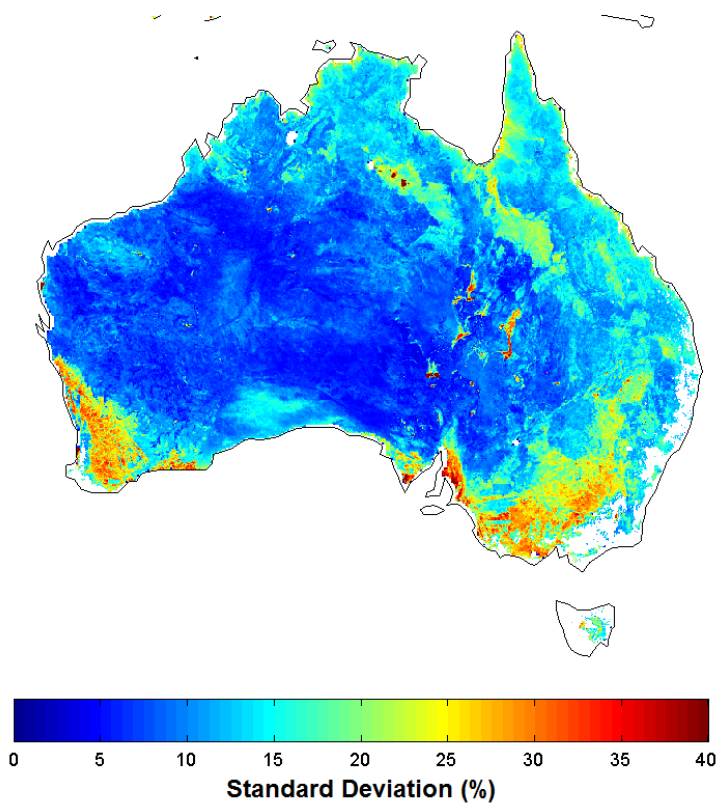
Figure 5: Temporal standard deviation of estimated degree of curing (DOC) map from 4 July 2002 to 26 June 2011.
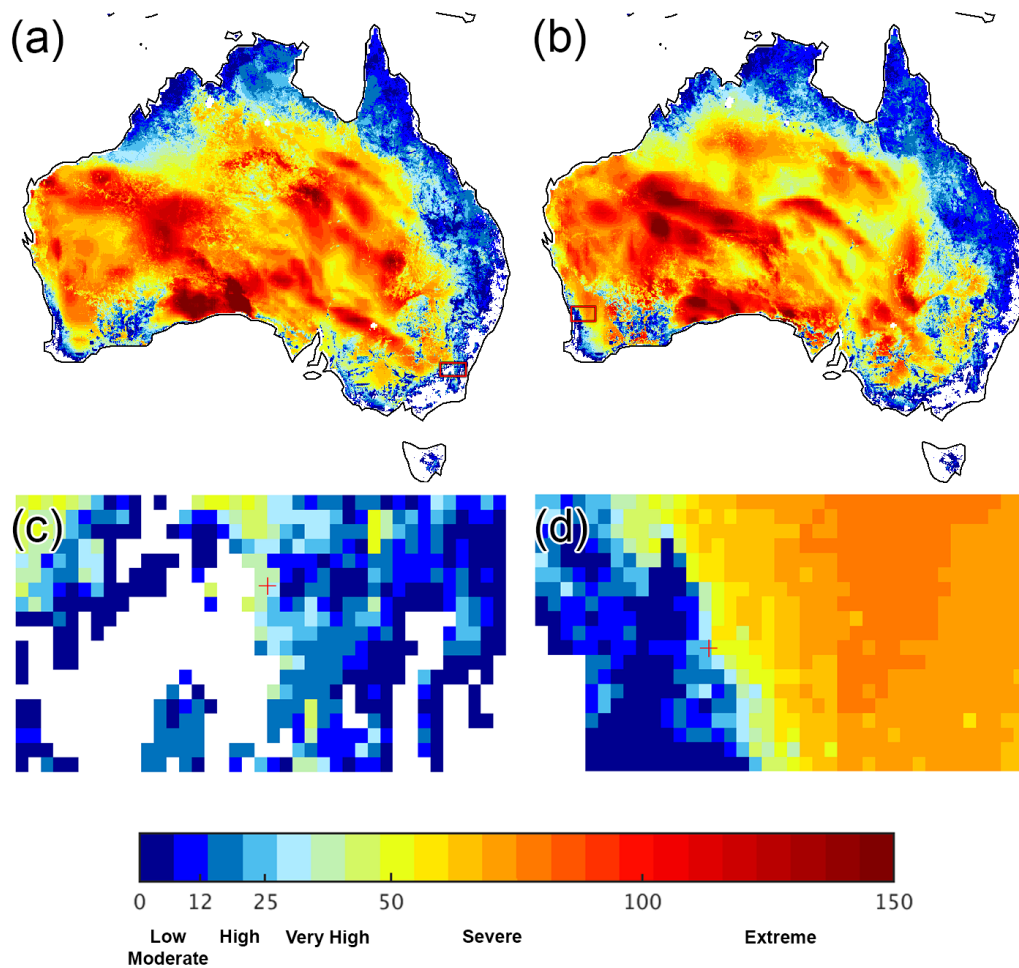
Figure 6: Maximum estimated Grassland Fire Danger Index (GFDI) for summer (December, January, February) of 2002—2003 (a) and 2009—2010 (b). Both zoomed areas marked with red bounding boxes for (a) and (b) are shown in (c) and (d), respectively. The fires locations for Canberra fire (c) and Toodyay fire (d) are marked with red crosshair. Forest areas are masked out in white.
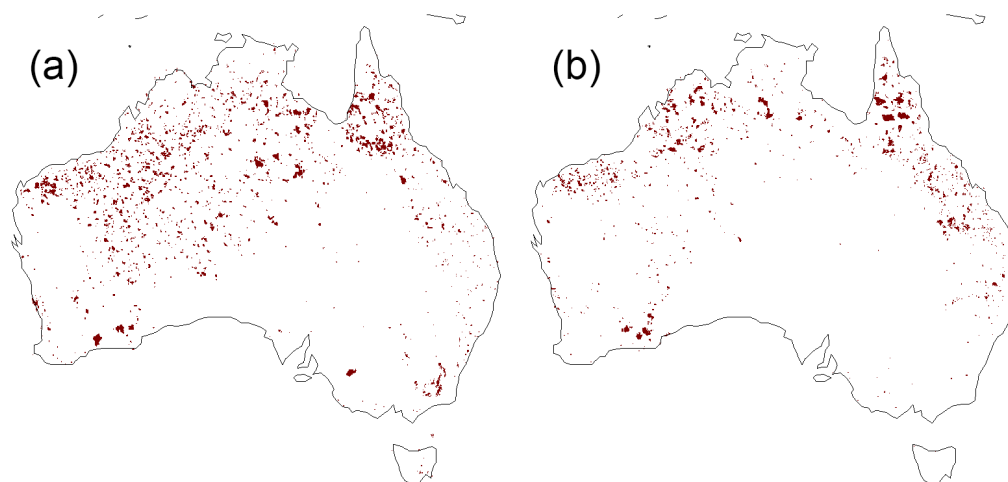
Figure 7: MCD64A1 burned area map (Ruiz et al., 2014) during summer (December, January, February) 2002—2003 (a) and 2009—2010 (b) with forest areas masked out.
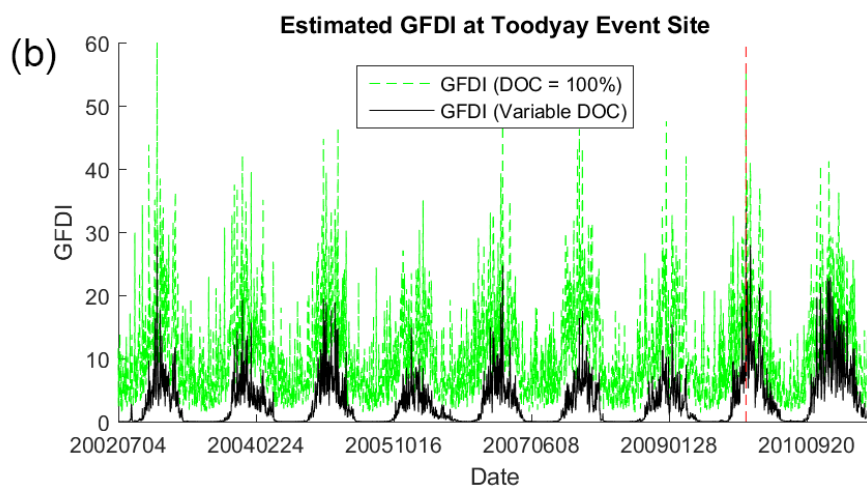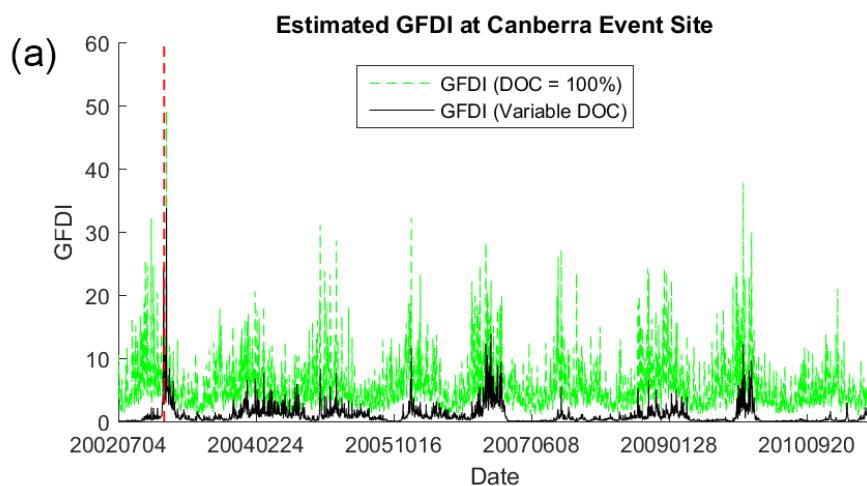
Figure 8: Grassland Fire Danger Index (GFDI) time series plot at Weston Creek, ACT, from July 2002 to June 2011 (a) and at Toodyay, WA, from July 2002 to June 2011 (b) where the vertical dash line indicates the date of fire event on 18 January 2003 for Canberra fire and on 29 December 2009 for Toodyay fire. Solid black line is estimated GFDI time series computed from estimated degree of curing (DOC), whereas green dash line is GFDI time series computed from constant DOC at 100 %.
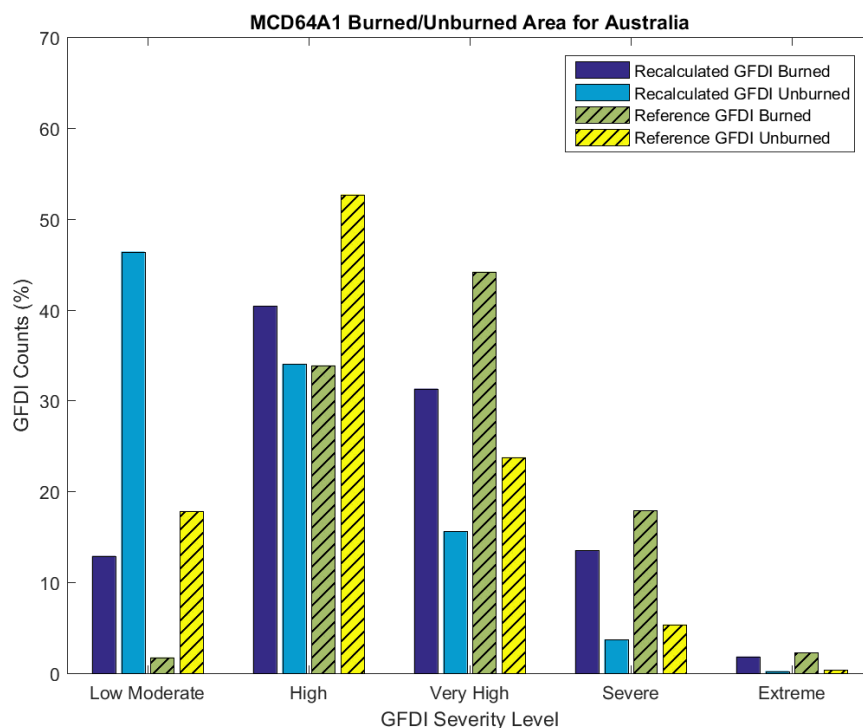
Figure 9: Grassland Fire Danger Index (GFDI) severity level histograms at burned and unburned areas over Australia during 4 July 2002 to 26 June 2011 where the dark and light blue shaded bars are recalculated GFDI with satellite estimated variable degree of curing (DOC), while the green and yellow shaded with diagonal hatch bars are reference GFDI with constant DOC at 100 %.

Table 1: Calibration and evaluation of satellite based degree of curing (DOC) model derived from Vegetation Optical Depth (VOD) and Normalised Difference Vegetation Index (NDVI). Existing estimated DOC models, Method B (Newnham et al., 2010) and MapVic (Martin et al., 2015), evaluations are also listed below.

DOC-VOD-NDVI Estimated Curing Model Calibration and Evaluation								
				Fitting Coefficient				**No. of Sites (Used/ All)**
Model	**r²**	**P-Value**	**RMSE (%)**	**x1**	**x2**	**x3**	**x4**	
DOC-VOD-NDVI Calibration	0.672	0.000	13.396	145.565	0.000	-260.817	137.194	5/23
DOC-VOD-NDVI Evaluation	0.551	0.000	15.254	-	-	-	-	23/23
Method B	0.611	0.000	14.438	-	-	-	-	23/23
MapVic	0.435	0.000	19.801	-	-	-	-	23/23

30

Table 2: Referenced and recalculated Grassland Fire Danger Index (GFDI) severity and burned—unburned area contingency table for satellite based degree of curing (DOC) derived from Vegetation Optical Depth (VOD) and Normalised Difference Vegetation Index (NDVI). Reference GFDI is computed from constant DOC at 100 %, while recalculated GFDI is computed from satellite based DOC.

		Reference GFDI		Recalculated GFDI	
		MCD64A1 No. of Pixels			
		Burned	Unburned	Burned	Unburned
GFDI Severity	High or above	2916	447425180	2271	288523884
	Low Moderate	399	417954158	1044	576855454

	Reference GFDI	Recalculated GFDI
True Positive Rate	0.8796	0.6851
False Positive Rate	0.5170	0.3334
Accuracy	0.4830	0.6666

30

Table 3: Recalculated Grassland Fire Danger Index (GFDI) severity and burned—unburned area contingency table for degree of curing (DOC) computed with Method B (Newnham et al., 2010) and MapVic (Martin et al., 2015) model. Reference GFDI is computed from constant DOC at 100 %, while recalculated GFDI is computed from satellite based DOC.

		Method B GFDI		MapVic GFDI	
		MCD64A1 No. of Pixels			
		Burned	Unburned	Burned	Unburned
GFDI Severity	High or above	311	131271221	2448	333457942
	Low Moderate	3005	717643041	866	512701649

	Method B GFDI	MapVic GFDI
True Positive Rate	0.0938	0.7387
False Positive Rate	0.1546	0.3941
Accuracy	0.8454	0.6059

30

Appendix A: List of Varaibles

- C – degree of curing (%)
- $C_{\text{Method B}}$ – estimated degree of curing using Method B model (%) (Newnham et al., 2011)
- C_{MapVic} – estimated degree of curing using MapVic model (%) (Martin et al., 2015)
5
- GVMI – global vegetation monitoring index (unitless)
- $f(C)$ – curing factor (unitless)
- H_{3pm} – daily relative humidity at 3 pm (%)
- $NDVI_{max}$ – maximum NDVI value over a specific time range used for calculating relative greenness (unitless)
- $NDVI_{min}$ – minimum NDVI value over a specific time range used for calculating relative greenness (unitless)
10
- Q – fuel load (kg m^{-2})
- RG – relative greenness (unitless)
- T_{max} – dry bulb or daily maximum temperature (° C)
- V_{max} – daily maximum wind speed (km h^{-1})
- x_1 – coefficient in the linear regression equation
15
- x_2 – coefficient in the linear regression equation
- x_3 – coefficient in the linear regression equation
- x_4 – coefficient in the linear regression equation
- ρ_1 – spectral reflectance measurements obtained from 620 to 670 m^{-6} region (unitless)
- ρ_2 – spectral reflectance measurements obtained from 841 to 876 m^{-6} region (unitless)
20
- ρ_6 – spectral reflectance measurements obtained from 1628 to 1652 m^{-6} region (unitless)

Appendix B: List of Acronyms

- AMSR-E (Advanced Microwave Scanning Radiometer – Earth Observing System) – one of the sensors aboard Aqua satellite; a passive microwave radiometre; stop rotating on 4 October 2011
- AMSR2 (Advance Microwave Scanning Radiometer 2) – one of the sensors aboard JAXA's GCOM-W1 satellite; a
25 passive microwave radiometre; currently operating
- AVHRR (Advanced Very High Resolution Radiometer) – a radiation detection that used for determining cloud cover and surface temperature
- AWAP (Australian Water Availability Project) – a state and trend of the terrestrial water balance monitoring project in Australia
30
- DOC (Degree of Curing) – a percentage measurement of dead material in grassland fuel complex
- ECMWF (European Centre for Medium–Range Weather Forecasts) – independent, intergovernmental organisation producing global numerical weather forecasts
- ERA–Interim – a global reanalysis climate dataset from 1979 to present
- LPRM (Land Parameter Retrieval Model) – a radiative transfer model for solving surface soil moisture and vegetation
35 optical depth from microwave observation
- Modified Mark 4 McArthur's Grassland Fire Danger Index (GFDI) – fire danger index for grassland ecosystem developed and used in Australia
- MCD12C1 – 2010 MODIS land cover type product (University of Maryland scheme)
- MCD45A1 – daily MODIS burned area product

- MCD64A1 – daily MODIS burned area product

- MOD09A1 – 8 day MODIS reflectance product on board Terra satellite

- MODIS (Moderate Resolution Imaging Spectroradiometer) – key instrument abroad Terra and Aqua satellites acquiring data in 36 spectral bands

- NDVI (Normalised Difference Vegetation Index) – optical based satellite product used as proxy for vegetation greenness

- NCI (National Computational Infrastructure) – Australia's highly integrated and high performance research computing environment

- NOAA (National Oceanic and Atmospheric Administration) – United States government agency working on daily
10   weather forecasts and climate monitoring

- P-Value – the significant of the results in a statistics hypothesis test where strong evidence against the null hypothesis is indicates by low p-value

- r^2 (R-Squared) – a statistical measurement of the closeness of the data to the fitted regression line

- RFI (Radio Frequency Interference) – interference in microwave based satellite product (VOD in this case) due to
15   wireless transmission, causing erroneous values in the affected grid pixels

- RMSE (Root Mean Square Error) – differences between the values estimated by a model and the observed values

- USGS (United States Geological Survey) – the United States government's scientific agency studying the landscape, natural resources, and natural hazards of the United States

- VOD (Vegetation Optical Depth) – microwave based satellite product used as proxy for vegetation moisture